Meissner transport current in flat films of arbitrary shape and a magnetic trap for cold atoms

2010 Supercond. Sci. Technol. 23 065003

(http://iopscience.iop.org/0953-2048/23/6/065003)

Supercond. Sci. Technol. **23** (2010) 065003 (7pp) doi:10.1088/0953-2048/23/6/065003

Meissner transport current in flat films of arbitrary shape and a magnetic trap for cold atoms

Vladimir Sokolovsky[1], **Leonid Prigozhin**[2] **and Valery Dikovsky**[1]

[1] Physics Department, Ben-Gurion University of the Negev, Beer-Sheva, 84105, Israel
[2] Department of Solar Energy and Environmental Physics, Blaustein Institutes for Desert Research, Ben-Gurion University of the Negev, Sede Boqer Campus, 84990, Israel

E-mail: sokolovv@bgu.ac.il, leonid@bgu.ac.il and dikovsky@bgu.ac.il

Received 21 January 2010
Published 21 April 2010
Online at stacks.iop.org/SUST/23/065003

Abstract
The use of superconducting films in the Meissner state reduces the level of noise in micro- and nanochips. Here we present a numerical scheme for computing the Meissner transport current distribution in superconducting films of arbitrary shape, including multiply connected films. The scheme is used for simulating a 3D magnetic trap for cold atoms. Our algorithm is easily generalized for computing the Meissner–London distribution of transport current.

(Some figures in this article are in colour only in the electronic version)

1. Introduction

Superconducting thin films are used in fault current limiters, superconducting quantum interference devices (SQUIDs), bolometers, A/D and D/A converters, etc (see [1] and the references therein). Recently, much interest has been attracted to the development of atom chips [2–9] in which thin superconducting films generate magnetic field traps for cold atoms, e.g. ^{87}Rb at micro-kelvin temperatures [10, 11]. Such chips are regarded a powerful tool for generating Bose–Einstein condensates and subsequent coherent manipulation of the quantum state of trapped atoms. Atomic interferometry and quantum gate implementation are potentially important applications of the atomic traps; the traps also enable researchers to carry out fundamental studies of atom–surface interactions, e.g. the Casimir–Polder force and spin decoherence of atoms near dielectric bodies, to probe local irregularities of magnetic and electric fields near conductive films using trapped atoms, etc (see [2–11] and the references therein).

An advantage of using superconductors is in the huge reduction of noise: according to estimates [5], the noise in an atom chip based on superconducting wires or films in the mixed state is about two orders lower than if the wires are in the normal state [12]. The remaining noise is then produced mainly by vortex motion in a superconductor and, as was shown experimentally, keeping the superconductor in the vortex-less Meissner state leads to a further two orders of magnitude decrease of noise [13–15].

Magnetic fields, generated in such micro- and nanodevices, are determined by the current distribution in superconducting films. Analytically, the distribution of screening current was found (both for the Meissner and mixed states) only for simple film geometries, like an infinitely long strip, disc or ring [16–18]. For films of arbitrary shape several numerical algorithms have been proposed for the mixed state (see, e.g., [19, 20]) and also for the Meissner state [21]. The films in these works were assumed isolated and only the eddy currents induced by external magnetic field variations have been simulated; the only exception is the analytical solution for transport current in a straight infinitely long strip [16, 17]. Approximately, under the assumption that the field induced by the current leads can be neglected, the transport current has also been accounted for in [22, 23]. However, no general numerical algorithm for thin film problems with transport current, typical of many superconductivity experiments and applications, has been proposed yet even for films in the ideal Meissner state considered in our work.

An outline of this paper is as follows. We describe the mathematical model (section 2) and the finite element approximation employed (section 3), present numerical examples (section 4) and, finally, simulate the magnetic field in a magnetic trap built upon a Z-shaped superconducting film (section 5).

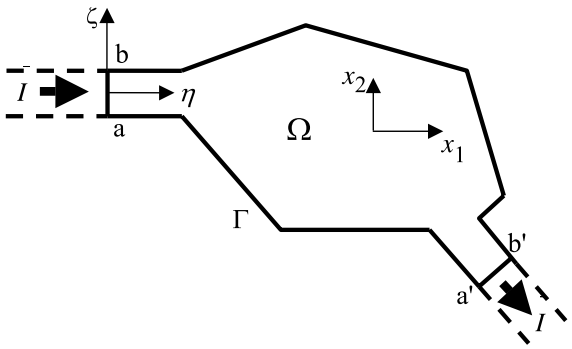

Figure 1. Thin film and two semi-infinite strip leads providing the transport current I. Numerically calculated current density in the film is matched to the analytically known distribution of current in the distant parts of the leads (dashed lines).

2. Mathematical model

Let a given transport current I be supplied to a superconducting film of arbitrary shape via two semi-infinite superconducting strip leads, see figure 1. We assume the film and strip thickness, d, is small compared to the width of each strip and to the characteristic size of the film midsection, lying in the plane $z = 0$. Hence, see [17], we can replace the real current distribution $\vec{j}$ by distribution of the sheet current $\vec{J}(x) = \int_{-d/2}^{d/2} \vec{j}(x, z)\,\mathrm{d}z$, where $x = (x_1, x_2)$. The superconductors are supposed to be in the ideal Meissner state, which means the magnetic field is completely expelled from their interior.

Our further assumptions are that, at least sufficiently far from the film, (i) these strips are also far from each other and (ii) at $z = 0$, the normal-to-strip component of the known applied external field is close to uniform: $H_{\mathrm{ext},z}(x) \approx H_0$. Hence, far from the film, the Meissner distribution of current in these strips is close to the analytical solution [16]: the current has only one component (along the strip) and is determined as

$$J_\eta(\zeta) = \frac{I/\pi - 2\zeta H_0}{\sqrt{w^2 - \zeta^2}}, \tag{1}$$

where the axes ζ, η are across and along the strip, respectively (figure 1), and w is half of the strip width. This allows us to limit our consideration only to a finite 2D domain Ω which contains the film and a sufficiently long part of each strip. The magnetic fields $H_{\mathrm{e}1,z}(x)$ and $H_{\mathrm{e}2,z}(x)$ produced in domain Ω by the two cutoff semi-infinite strips (dashed lines in figure 1) are calculated and added to the given external field:

$$H_\mathrm{e} = H_{\mathrm{ext},z} + H_{\mathrm{e}1,z} + H_{\mathrm{e}2,z}.$$

Using the Biot–Savart law we obtain the following presentation for the field of the semi-infinite strip $[-w, w] \times (-\infty, 0]$ in strip-related coordinates (ζ, η):

$$H_{\mathrm{e}i,z}(\zeta, \eta) = \frac{1}{4\pi} \int_{-w}^{w} \frac{J_\eta(\zeta')}{\zeta - \zeta'} \left[1 - \frac{\eta}{\sqrt{(\zeta - \zeta')^2 + \eta^2}}\right] \mathrm{d}\zeta', \quad i = 1, 2. \tag{2}$$

Note that for any $\eta > 0$ and ζ' close to ζ we have

$$\frac{1}{\zeta - \zeta'} \left[1 - \frac{\eta}{\sqrt{(\zeta - \zeta')^2 + \eta^2}}\right] \approx \frac{\zeta - \zeta'}{2\eta^2}.$$

Hence, the only singularity in (2) is the integrable singularity of $J_\eta(\zeta')$ at $\zeta' = \pm w$. The field $H_{\mathrm{e}i,z}(\zeta, \eta)$ quickly decreases with the distance from the strip end and, at a distance of several strip widths, becomes negligibly small (figure 2(a)).

For simplicity, we assume at first the domain Ω is simply connected. The boundary Γ of domain Ω contains the cuts of two strip contacts, a–b and a′–b′, where we set, using (1), the normal component J_n of sheet current density $\vec{J}$ as $J_\mathrm{n} = -J_\eta$ and $J_\mathrm{n} = +J_\eta$, respectively; on the rest of the boundary $J_\mathrm{n} = 0$.

At a point x on the plane $z = 0$ the sheet current $\vec{J}$ induces the magnetic field normal to this plane:

$$H_i(x)\vec{e}_z = \frac{1}{4\pi} \int\int_\Omega \vec{\nabla} \left(\frac{1}{|x - x'|}\right) \times \vec{J}(x')\,\mathrm{d}x', \tag{3}$$

and, in the ideal Meissner state, everywhere in Ω:

$$H_\mathrm{e} + H_i = 0. \tag{4}$$

Since current density satisfies $\vec{\nabla} \cdot \vec{J} = 0$ in Ω, it is possible to introduce a stream function g such that

$$\vec{J} = \vec{\nabla} \times g \qquad \text{in } \Omega \tag{5}$$

and, thereby, $\partial_\tau g = J_\mathrm{n}$ on Γ. Here $\vec{\nabla} \cdot \vec{V} = \partial V_1/\partial x_1 + \partial V_2/\partial x_2$ and $\vec{\nabla} \times f = (\partial f/\partial x_2, -\partial f/\partial x_1)$ are the usual 2D divergence and curl operators, respectively, and τ is the counter-clockwise length parameterization of Γ. The boundary condition makes sense because $\oint_\Gamma J_\mathrm{n}\,\mathrm{d}\tau = 0$; see [22, 23] for a discussion on the properties of the stream function. Substituting (5) into (3), we can rewrite (4) as the following integral equation for the stream function:

$$H_\mathrm{e}(x) - \frac{1}{4\pi} \int\int_\Omega \vec{\nabla}' g(x') \cdot \vec{\nabla} \left(\frac{1}{|x - x'|}\right) \mathrm{d}x' = 0 \quad \text{in } \Omega. \tag{6}$$

Equation (6) and the boundary condition $\partial_\tau g = J_\mathrm{n}$ determine the stream function up to an additive constant. To fix this constant, let us set $g(x^0) = 0$ at some point x^0 on Γ, define $\Psi(x) = \int_{\Gamma(x^0, x)} J_\mathrm{n}\,\mathrm{d}\tau$ for any x on Γ and rewrite the boundary condition as

$$g|_\Gamma = \Psi. \tag{7}$$

Below we set $g = 0$ on the part a–a′ of the boundary Γ, hence $g = I$ on the part b–b′, and, integrating J_η in ζ, obtain values of g also on the parts a–b and a′–b′ of Γ.

The ideal Meissner state model is inappropriate if the film thickness d is less than the London penetration depth λ. In such a case equation (4) should be replaced by the equation $H_\mathrm{e} + H_i = -\Lambda(\vec{\nabla} \times \vec{J})_z = \Lambda \nabla^2 g$, where $\Lambda = \lambda^2/d$ (see [22, 23]). Although in this paper we limit our consideration to the ideal Meissner case $\Lambda = 0$, taking the Laplacian term into account in equation (6) is straightforward and would involve only a minor modification of our numerical algorithm.

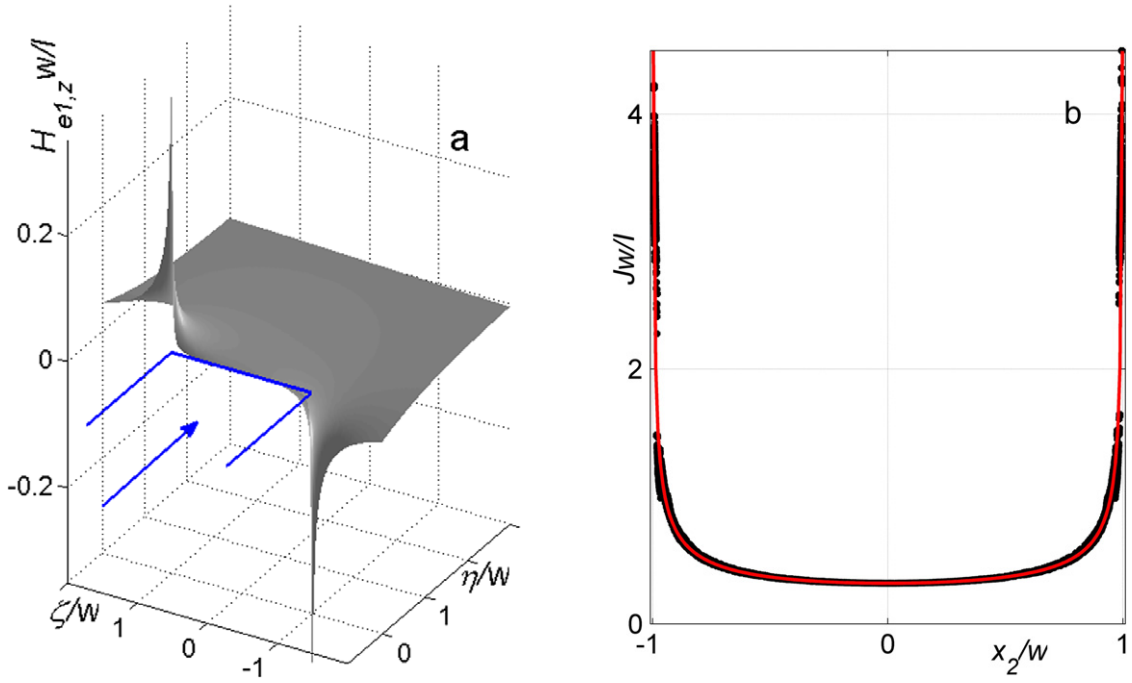

Figure 2. (a) Magnetic field $H_{e1,z}(\zeta, \eta)$ induced by the Meissner transport current in half of an infinite strip; the solid line and the arrow indicate strip position and current direction, respectively. (b) Sheet current density, accuracy test: the numerical solution (black dots) obtained for the domain $\Omega = [-5w, 5w] \times [-w, w]$ cut out of an infinite strip and the analytical one (red line); the finite element mesh is refined near the domain boundary.

We note also that the analytical solution (1), describing the current density in strips far away from the film, can be replaced by any other known distribution, e.g. if the strips are close to each other, so their inter-influence is significant.

The formulation (6) and (7) should be modified also if the film contains several holes $\Omega_k, k = 1, \ldots, K$. We are still able to use the stream function satisfying (6) and also the condition (7) on the *outer* domain boundary Γ, which is the boundary of $\Omega \bigcup (\bigcup_{k=1}^{K} \bar{\Omega}_k)$. On the boundary Γ_k of each hole Ω_k (the *inner* boundaries of Ω) the normal component of current density, J_n, is zero, so the stream function should be constant:

$$g|_{\Gamma_k} = c_k, \qquad k = 1, \ldots, K. \tag{8}$$

By the Faraday law

$$\oint_{\Gamma_k} \vec{E} \cdot \mathrm{d}\vec{\tau}_k = -\frac{\mathrm{d}}{\mathrm{d}t} \int\int_{\Omega_k} (H_e + H_i)\, \mathrm{d}x$$

and, since the tangential component of the electric field on the boundary of a superconductor is zero, the integral $\int\int_{\Omega_i} (H_e + H_i)\, \mathrm{d}x$ must be a time-independent constant. In our examples below we assume that, initially, the magnetic field is zero, so additional equations, needed to determine K constants c_k in (8), can be written as

$$\int\int_{\Omega_k} H_e\, \mathrm{d}x - \frac{1}{4\pi} \int\int_{\Omega} \vec{\nabla}' g(x') \cdot \left(\int\int_{\Omega_k} \vec{\nabla} \left[\frac{1}{|x - x'|} \right] \mathrm{d}x \right) \mathrm{d}x' = 0 \tag{9}$$

for $k = 1, \ldots, K$.

3. Finite element approximation

Let T be a partition of domain Ω into triangular finite elements $\sigma \in T$ and N be the set of nodes (element vertices). We seek an approximation to the stream function as a linear combination of piecewise linear basis functions, $g(x) = \sum_{i \in N} g_i \varphi_i(x)$, where φ_i is continuous, linear on each finite element, equal to 1 at the node i, and zero at all other nodes. The set of nodes N can be presented as $N^\Omega \bigcup N^\Gamma \bigcup (\bigcup_{k=1}^{K} N^{\Gamma_k})$, where N^Ω denotes the set of all nodes inside the domain Ω, N^Γ is the set of all nodes on the boundary Γ and N^{Γ_k} are the sets of nodes on the hole boundaries Γ_k. Multiplying equation (6) by φ_j, $j \in N^\Omega$, and integrating, we obtain linear algebraic equations:

$$\int\int_{\Omega} H_e \varphi_j\, \mathrm{d}x - \frac{1}{4\pi} \sum_{i \in N} g_i \int\int_{\Omega} \int\int_{\Omega} \vec{\nabla}' \varphi_i(x') \cdot \vec{\nabla} \left(\frac{1}{|x - x'|} \right) \varphi_j(x)\, \mathrm{d}x\, \mathrm{d}x' = 0, \qquad j \in N^\Omega.$$

Since φ_j is zero on the boundary of Ω, making use of the Green formula yields

$$b_j + \sum_{i \in N} A_{ji} g_i = 0, \qquad j \in N^\Omega, \tag{10}$$

where $b_j = \int\int_{\Omega} H_e \varphi_j\, \mathrm{d}x$ and $A_{ij} = \frac{1}{4\pi} \int\int_{\Omega} \int\int_{\Omega} \frac{\vec{\nabla}' \varphi_i(x') \cdot \vec{\nabla} \varphi_j(x)}{|x - x'|}\, \mathrm{d}x\, \mathrm{d}x'$.

Note that by (7) g_i is known for every $i \in N^\Gamma$. Furthermore, by (8), for each $i \in N^{\Gamma_k}$, g_i is equal to the same unknown constant c_k. Taking this into account, we rewrite

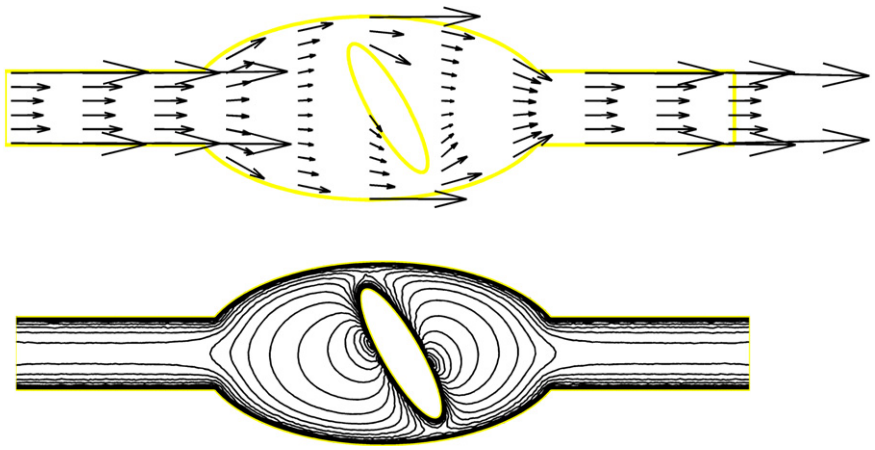

Figure 3. Current density in a multiply connected film. Top: the vector field $\vec{J}$; bottom: level contours of $\ln(J)$.

equation (10) as

$$\sum_{i\in N^\Omega} A_{ji} g_i + \sum_{k=1}^{K} c_k \left(\sum_{i\in N^{\Gamma_k}} A_{ji} \right) = -b_j - \sum_{i\in N^\Gamma} A_{ji}\Psi_i, \quad j \in N^\Omega, \tag{11}$$

where Ψ_i is the value of Ψ at the boundary node $i \in N^\Gamma$. In a similar way, using (7)–(9) we derive

$$\sum_{i\in N^\Omega} \hat{A}_{ji} g_i + \sum_{k=1}^{K} c_k \left(\sum_{i\in N^{\Gamma_k}} \hat{A}_{ji} \right) = -\hat{b}_j - \sum_{i\in N^\Gamma} \hat{A}_{ji}\Psi_i, \quad j = 1,\ldots,K, \tag{12}$$

where $\hat{A}_{ij} = -\frac{1}{4\pi}\int\int_\Omega \vec{\nabla}'\varphi_i(x')\cdot(\int\int_{\Omega_j} \vec{\nabla}\frac{1}{|x-x'|}\,\mathrm{d}x)\,\mathrm{d}x'$, $\hat{b}_j = \int\int_{\Omega_j} H_\mathrm{e}\,\mathrm{d}x$.

Since gradients of the basis functions are constant on each finite element, assembling the matrix $\{A_{ij}\}$ is based on the approximation of integrals

$$\int\int_{\sigma_m}\int\int_{\sigma_\mathrm{n}} \frac{1}{|x-x'|}\,\mathrm{d}x\,\mathrm{d}x' \tag{13}$$

for each pair of finite elements $\sigma_m, \sigma_\mathrm{n} \in T$ and, to assemble $\{\hat{A}_{ij}\}$, the integrals

$$\int\int_{\sigma_m}\int\int_{\Omega_j} \vec{\nabla}\frac{1}{|x-x'|}\,\mathrm{d}x\,\mathrm{d}x' \tag{14}$$

have to be calculated for all $\sigma_m \in T$, $j = 1,\ldots,K$. Some of these integrals are singular or weakly singular and, although many approaches exist, their accurate calculation remains non-trivial. The integration procedures employed in our computations are described in the appendix.

We note that the matrix of the linear algebraic system (11) and (12) is full and, using a personal computer, we were unable to perform computations on finite element meshes with more than about 5000 nodes due to the memory limitation. Implementation of the fast multipole method or a similar approach would significantly complicate our simple algorithm but can remove this constraint and make the scheme more efficient.

4. Solution of model problems

Since modeling Meissner's state for thin films in an external magnetic field has already been performed, see [21–23], in the examples below we consider only the case of transport current and assume the external field $H_{\mathrm{ext},z}$ is zero. Of course, in the general case, the solution is the sum of solutions to problems with $I \neq 0$, $H_{\mathrm{ext},z} = 0$ and $I = 0$, $H_{\mathrm{ext},z} \neq 0$.

As a test for our computations, we cut the infinitely long strip $[-\infty,\infty] \times [-w, w]$ at $x_1 = \pm 5w$, set $\Omega = [-5w, 5w] \times [-w, w]$ and compare the computed current density in this domain to the analytical solution (1) for the infinite strip with $H_0 = 0$ (the red line in figure 2(b)). The approximate current density J in our scheme is constant inside each finite element; its values are related to the centers of elements and shown on the same plot as black dots; the approximation is satisfactory.

In this and other simulations below, the finite element mesh contained about 10 000 elements and slightly more than 5000 nodes; the mesh was refined near the domain boundary to better approximate singular current density distributions typical of the Meissner state in thin films.

Computing current density distribution in multiply connected superconducting films is needed for films with natural or artificially created defects [24, 25], SQUIDs [22, 23], some types of atom chips [26], etc. As an example, we present the calculated current density in a film with one hole (figure 3). Here the length of the remaining strip parts was $7w$. This is enough, since our calculation shows that the current distribution is close to the distribution in an infinitely long strip at a distance $5w$ from the film.

5. Magnetic trap simulation

In the adiabatic approximation, trapping of cold atoms occurs in the vicinity of the minimum of the magnetic field modulus, the magnetic potential $H = |\vec{H}|$, see [11]. Here we consider a magnetic trap based on a Z-shaped superconducting thin film in the Meissner state (figure 4); films of such a shape have been used for atom trapping in [2, 27]. For this design, the

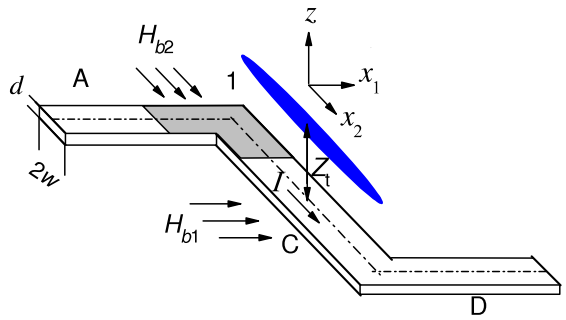

Figure 4. Magnetic trap for cold atoms (a sketch). The gray region is the area of numerical simulation. Each side of the angle equals $10w$. The atom cloud is shown as the blue domain.

minimum of the magnetic field modulus, $H = 0$, at a chosen trap height $z = z_t$, is achieved by applying an external bias field H_{b1} parallel to the x_1 axis. This field is directed opposite to the current-induced field and cancels it at the chosen height. The zero value of H anywhere in the trap is, however, undesirable because of the Majorana instability. Hence, a small bias field H_{b2}, parallel to the x_2 axis, is additionally applied [10, 11]. The influence of the parallel-to-film bias fields on the sheet current can be neglected and, since $H_{\text{ext},z} = 0$, the current distribution remains determined by the transport current alone.

Typically, the strips A and D in experiments are at least $100w$ long and part C is about $40w$ or longer [10, 11]. At a distance of several strip widths from the film corners the current density is well described by the analytical solution for an infinite strip and, due to problem symmetry, it is sufficient to find the current density near one of the two strip corners. In our simulations the computational domain Ω (shown as the gray region in figure 4) contained $10w$-long parts of strips A and C near corner 1. It has been found that 'rounding' the film corner (see figure 5) weakens the singularity of the current density and is, therefore, desirable. Computed current density (figure 5) is the strongest near the inner side of the angle, becomes much smaller near its outer side and converges to the analytical solution [16, 17] as the distance from the corner increases.

Substituting $\vec{J} = \vec{\nabla} \times g$ into the Biot–Savart law, we find the induced magnetic field at a point $r = (x, z)$:

$$\vec{H}_i(r) = \frac{1}{4\pi} \int\int_{\Omega} \{[-\partial_{x_1'} g(x')z, -\partial_{x_2'} g(x')z, \{\partial_{x_1'} g(x')(x_1 - x_1') + \partial_{x_2'} g(x')(x_2 - x_2')\}]\}\{|r - r'|^3\}^{-1} \mathrm{d}x',$$

where $r' = (x', 0)$. For our piecewise linear approximation of the stream function g, this field calculation boils down to computing the integrals of functions $1/|r - r'|^3$, $(x_1 - x_1')/|r - r'|^3$ and $(x_2 - x_2')/|r - r'|^3$ over each finite element (see the appendix).

The ability of a magnetic trap to hold cold atoms depends mainly on the atom temperature and the trap depth, i.e. the depth of the magnetic potential well (see [10, 11]). Three level surfaces of the potential, $H - H_{b2}$, built for the calculated induced magnetic field, are shown in figure 6 (the bias field H_{b1} is such that the trap axis is at the height w above the film). As an example, let us consider a micro-chip based on a thin niobium strip of width $2w = 10$ μm (see [6]). The applied transport current, 20 mA, is much less than the critical value, about 0.45 A at 4.2 K (this guarantees the Meissner state of the strip). The isopotential surfaces presented in figure 6 correspond then to the potential values of 0.76 G (green), 1.16 G (red) and 1.56 G (yellow). Such potentials are sufficient to hold ^{87}Rb atoms up to the atom temperatures of about 13, 19 and 25 μK, respectively (the atom temperature of 1 μK requires a potential well depth of 0.06 G for reliable trapping [6]). Since typical atom temperatures in experiments are several micro-kelvins [6, 10, 11], our simulation confirms the ability of atom chips, based on thin Z-shaped superconducting films in the Meissner state, to trap cold atoms of a sufficiently wide temperature range.

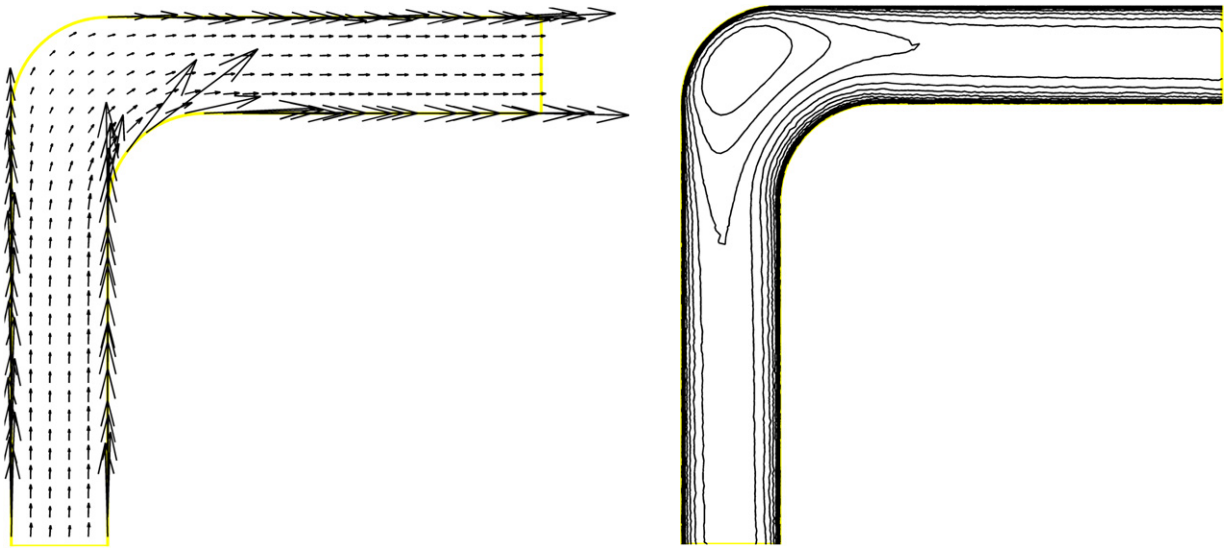

Figure 5. Sheet current density in the corner of a Z-shaped superconducting film of an atom chip. Left—the vector field $\vec{J}$ (the yellow line is the boundary Γ); right—the contour plot of $\ln(J)$.

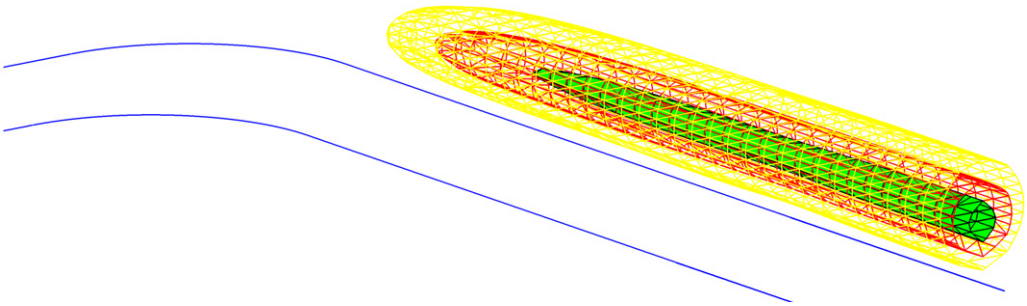

Figure 6. Numerical simulation of magnetic trap (a part of the trap near the film corner is shown). For the chosen bias field $H_{b1} = 0.11I/w$ the trap axis is at the height $z_t \approx w$ above the film; at this axis $H = H_{b2} = 0.01I/w$. Isopotential surfaces of the trapping potential, $H - H_{b2}$, are shown for the following values: 0.015 (inner, green), 0.023 (intermediate, red) and 0.031 (outer, yellow) in I/w units.

6. Conclusion

A numerical method for computing the Meissner current density distribution in a thin superconducting film of arbitrary shape has been presented. Unlike the previous schemes, this method is applicable to problems with transport current. Simulation results were presented for simply and multiply connected superconducting films; we also modeled a 3D magnetic trap for cold atoms. The method can be easily adapted to the Meissner–London model, appropriate if the film thickness is of the order of or less than the London penetration depth.

Acknowledgments

VD and VS acknowledge the support of the German-Israeli Foundation for Scientific Research (GIF). The authors appreciate discussions with R Folman.

Appendix. Calculation of integrals

Accuracy of the numerical solution strongly depends on the treatment of a variety of singular and weakly singular integrals arising in our scheme; here we briefly describe the algorithms employed. The one-dimensional integrals (2) were regularized as

$$H_{ei,z}(\zeta,\eta) = \frac{1}{4\pi}\int_{-w}^{w} \frac{\mathrm{sgn}(\zeta-\zeta')J_\eta^\varepsilon(\zeta')}{\sqrt{(\zeta-\zeta')^2+\varepsilon^2}} \times\left[1-\frac{\eta}{\sqrt{(\zeta-\zeta')^2+\eta^2}}\right]\mathrm{d}\zeta',$$

where $J_\eta^\varepsilon(\zeta) = (I/\pi d - 2\zeta H_0)/\sqrt{w^2-\zeta^2+\varepsilon^2}$ and computed (for $\varepsilon = 10^{-7}w$) with a given accuracy by means of a standard Matlab adaptive quadrature *quad*.

The double-surface integrals (13) are most singular for coinciding triangles of integration, i.e. if $m = n$. In this case an exact analytical expression for (13) is known [28]. The integrals remain singular if the triangles have a common edge or node; these integrals are called weakly singular if the triangles are separated but close. In these cases we used an analytical expression [29] for the inner integral (over σ_n). The resulting nonsingular function was then integrated numerically over the second element, σ_m, using the seven-point Gauss formula for triangles. Finally, for distantly separated elements the integrals were approximated as $|\sigma_n||\sigma_m|/r_{mn}$, where r_{mn} is the distance between the element centers.

In the double-surface integrals (14) the singularity is stronger but element σ_m can be at most adjacent to the domain Ω_j. As a result of triangulation, the domain is approximated by a polygon and we performed integration over it analytically, using the method [30, 31] applicable for arbitrary polygons. Numerical integration of the resulting nonsingular function over σ_m was also based on the seven-point Gauss formula.

The integrals of functions $1/|r-r'|^3$ and $(x-x')/|r-r'|^3$, needed to compute the magnetic field in section 5, are nonsingular ($z > 0$). Most of these integrals are easily approximated using the same Gauss formula for triangles. However, for small values of z the integrals over finite elements close to the observation point r become weakly singular and the analytical integration formulae [30, 31] are then preferable.

References

[1] ter Brake H J M *et al* 2006 SCENET roadmap for superconductor digital electronics *Physica* C **439** 1–41
[2] Nirrengarten T *et al* 2006 Realization of a superconducting atom chip *Phys. Rev. Lett.* **97** 200405
[3] Hufnagel C, Mukai T and Shimizu F 2009 Stability of a superconductive atom chip with persistent current *Phys. Rev.* A **79** 053641
[4] Muller T *et al* 2009 Trapping of ultra-cold atoms with the magnetic field of vortices in a thin film superconducting micro-structure arXiv:0910.2332 [physics.atom-ph]
[5] Nogues G *et al* 2009 Effect of vortices on the spin-flip lifetime of atoms in superconducting atom-chips *EPL* **87** 13002
[6] Dikovsky V, Sokolovsky V, Zhang B, Henkel C and Folman R 2009 Superconducting atom chips: advantages and challenges *Eur. Phys. J.* D **51** 247–59
[7] Cano D *et al* 2008 Impact of the Meissner effect on magnetic microtraps for neutral atoms near superconducting thin films *Phys. Rev.* A **77** 063408
[8] Cano D *et al* 2008 Meissner effect in superconducting microtraps *Phys. Rev. Lett.* **101** 183006
[9] Emmert A *et al* 2009 Microtraps for neutral atoms using superconducting structures in the critical state *Phys. Rev.* A **80** 061604
[10] Fortagh J and Zimmermann C 2007 Magnetic microtraps for ultracold atoms *Rev. Mod. Phys.* **79** 235–89

[11] Folman R, Kruger P, Schmiedmayer J, Denschlag J and Henkel C 2002 Microscopic atom optics: from wires to an atom chip *Adv. At. Mol. Opt. Phys.* **48** 263–356
[12] Hohenester U, Eiguren A, Scheel S and Hinds E A 2007 Spin-flip lifetimes in superconducting atom chips: Bardeen–Cooper–Schrieffer versus Eliashberg theory *Phys. Rev.* A **76** 033618
[13] Doenitz D, Straub R, Kleiner R and Koelle D 2004 Microscopic analysis of low-frequency flux noise in $YBa_2Cu_3O_7$ direct current superconducting quantum interference devices *Appl. Phys. Lett.* **85** 5938–40
[14] Dantsker E *et al* 1996 Reduction of $1/f$ noise in high-T_c dc superconducting quantum interference devices cooled in an ambient magnetic field *Appl. Phys. Lett.* **69** 4099–101
[15] Gail J, Muck M and Heiden C 1999 Depending of single vortices in niobium thin film dc superconducting quantum interference devices by rf demagnetization *IEEE Trans. Appl. Supercond.* **9** 3519–22
[16] Zeldov E, Clem J R, McElfresh M and Darwin M 1994 Magnetization and transport currents in thin superconducting films *Phys. Rev.* B **49** 9802–22
[17] Brandt E H and Indenbom M 1993 Type-II-superconductor strip with current in a perpendicular magnetic field *Phys. Rev.* B **48** 12893–906
[18] Babaei Brojeny A A and Clem J R 2003 Magnetic-field and current–density distribution in thin-film superconducting rings and disks *Phys. Rev.* B **68** 174514
[19] Schuster Th, Kuhn H and Brandt E H 1996 Flux penetration into flat superconductors of arbitrary shape: pattern of magnetic and electric field and current *Phys. Rev.* B **54** 3514–24
[20] Prigozhin L 1998 Solution of thin film magnetization problems in superconductivity *J. Comput. Phys.* **144** 180–93
[21] Brandt E H and Mikitik G P 2000 Meissner–London currents in superconductors with rectangular cross section *Phys. Rev. Lett.* **85** 4164–7
[22] Brandt E H 2007 Supercurrents and vortices in SQUIDs and films of various shapes *Physica* C **460–462** 327–30
[23] Brandt E H 2005 Thin superconductor and SQUIDs in perpendicular magnetic field *Phys. Rev.* B **72** 024529
[24] Vestgarden J I, Shantsev D V, Galperin Y M and Johansen T H 2008 Flux distribution in superconducting films with holes *Phys. Rev.* B **77** 014521
[25] Raedts S *et al* 2004 Flux pinning properties of holes and blind holes arranged periodically in a superconductor *Physica* C **404** 298–301
[26] Muller T *et al* 2008 Towards a guided atom interferometer based on a superconducting atom chip *New J. Phys.* **10** 073006
[27] Mukai T *et al* 2007 Persistent supercurrent atom chip *Phys. Rev. Lett.* **98** 260407
[28] Arcioni P, Bressan M and Perregrini L 1997 On the evaluation of the double surface integrals arising in the application of the boundary integral method to 3D problems *IEEE Trans. Microw. Theory Technol.* **45** 436–9
[29] Wilton D R *et al* 1984 Potential integrals for uniform and linear source distributions on polygonaland polyhedral domains *IEEE Trans. Antennas Propag.* **AP-32** 276–81
[30] Hodges R E and Rahmat-Samii Y 1997 The evaluation of MFIE integrals with the use of vector triangle basis functions *Microw. Opt. Technol. Lett.* **14** 9–14
[31] Gibson W C 2008 *The Method of Moments in Electromagnetics* (London: Chapman and Hall)